Rare Metal Materials and Engineering
Volume 50, Issue 1, January 2021
Available online at www.rmme.ac.cn

Science Press

Cite this article as: Rare Metal Materials and Engineering, 2021, 50(1): 0035-0042.

ARTICLE

First-Principles Calculation of Low Young's Modulus Ti-Mo-Sn Alloys for Biomedical Applications

Zhao Xi[1,2], Yu Sen[1,2], Zheng Jiming[3], Liu Hanyuan[1,2], Cheng Jun[1,2], Ma Xiqun[1,2]

[1] Northwest Institute for Nonferrous Metal Research, Xi'an 710016, China; [2] Shaanxi Key Laboratory of Biomedical Metal Materials, Xi'an 710016, China; [3] Northwest University, Xi'an 710069, China

Abstract: The density functional theory (DFT) implemented in Vienna Ab-initio simulation package (VASP) code was employed to investigate the β phase stability and elastic properties of Ti-xMo-Sn (x=1~5) alloys. The structural properties were investigated after geometrical optimization. The general elastic properties (such as bulk modulus B, shear modulus G, Young's modulus E) were estimated by Voigt-Reuss-Hill approximation. In addition, the valence electron criterion for design of low Young's modulus Ti-xMo-Sn alloys was proposed. The calculated cohesive energy indicates that Mo can increase the β phase stability of Ti-xMo-Sn alloys. The Pugh ratio B/G and Poisson's ratio v suggest that all these alloys exhibit ductile properties. For Ti-xMo-Sn alloys, the smaller tetragonal shear constant C' may induce the lower Young's modulus. Ti-3Mo-Sn possesses the lowest Young's modulus (48.47 GPa) and the best ductility, showing great potential for biomedical applications. The elastic anisotropy A of Ti-xMo-Sn alloys is sensitive to Mo concentration; the lowest Young's modulus always orients in the <100> crystallographic direction. In the end, total and partial DOS analysis was used to explain the calculated results.

Key words: biomedical Ti alloys; first-principles calculation; alloy design; low Young's modulus; elastic properties;

Ti-based alloys have attracted increasing attention and interest in the last decade owing to their potential biomedical applications, especially in load-bearing implants field. This is attributed to their high specific strength, excellent biocompatibility, corrosion resistance, fatigue resistance and low Young's modulus[1-4]. The commercial alloy Ti-6Al-4V has been widely used as orthopedic implants, while it's Young's modulus (~150 GPa) is significantly higher than that of natural bones (10~30 GPa), and the mismatched Young's modulus may cause "stress shielding" problem and lead to disuse atrophy of natural bone. Moreover, the alloying elements such as Al and V have been proved to be cytotoxic which may cause adverse tissue reaction[5]. Accordingly, recent research associated with this field has been mainly focused on design of novel Ti-based alloys which are compatible with surrounding living-tissue and human bone[6-8].

It is well known that Young's modulus is not sensitive to microstructure and depends more on the type of the crystal structure. Since the β-Ti alloys have similar Young's modulus to natural bone and the β-phase stabilizing elements (such as Nb, Mo, Ta, Zr, etc.) have been proven to be non-cytotoxic, the β-Ti alloys are considered to be desirable materials for biomedical applications. Previous studies indicated that Mo is the most effective β stabilizer which can maintain the β phase of Ti alloys at room temperature with only 10wt% addition while Sn can improve the low temperature ductility of Ti-Mo alloys[7]. In addition, many literatures have reported the martensitic transformation behavior (from β parent phase to α'' martensite phase) in Ti-Mo-Sn alloys, which is related to the superelastic and shape memory effect[9,10]. Such functional characteristics show important practical value in stent interventional therapy applications [11]. It is known that the cost of artificial joints is too high for many patients to afford,

Received date: June 25, 2020
Foundation item: Natural Science Basic Research Plan in Shaanxi Province of China (2018JM5145); Key Research and Development Program of Shaanxi (2019GY-151); National Natural Science Foundation of China (51801162, 51901193)
Corresponding author: Yu Sen, Ph. D., Professor, Northwest Institute for Nonferrous Metal Research, Xi'an 710016, P. R. China, Tel: 0086-29-86222297, E-mail: barbern@163.com

especially in poor areas. Replacing the high-cost alloying elements is the most effective approach to reduce the cost of biomedical Ti alloys. The price of Mo is only 1/8 of Co, 1/20 of V, and 1/2 of Nb, making it more attractive in the designing of low-cost biomedical Ti alloys. Based on the comprehensive advantages mentioned above, Ti-Mo-Sn alloys show great potential for biomedical applications and need to be better understood.

The first principles calculation based on density functional theory (DFT) is one of the most effective theoretical methods in material design[12,13]. It can exactly predict the β-phase stability and elastic properties of Ti alloys, and reveal the physical mechanism in comparison with conventional empirical methods such as e/a criterion[14] and Bo-Md method[15]. Many studies reported the mechanical properties and biocompatibility of multicomponent Ti-Mo alloys in experiment, especially in improving the process performance, while the theoretical physical mechanism of low elastic modulus is also important in biomedical Ti alloys design[16,17]. In addition, the classical "trial and error" way to obtain a desirable material needs a long period of time and is economically unfeasible in most cases, so it is quite necessary to use theoretical calculation methods for screening before pre-experiment.

In the present work, the β phase stability, elastic properties and electronic properties of Ti-xMo-Sn (x=1~5) alloys with Mo addition (6.25at%~31.25at%) were systematically investigated. In addition, the elastic modulus oriented in different crystal directions were investigated to estimate the anisotropy of Ti-xMo-Sn (x=1~5) alloys. We envision that this research will provide a theoretical basis for the composition design of Ti-Mo-Sn alloys.

1 Calculation Method

The geometry optimization, elastic and electronic properties of Ti-xMo-Sn (x=1~5) alloys were predicted by employing the Vienna Ab-initio simulation package (VASP) based on density functional theory (DFT)[18]. The projector augmented wave (PAW) was used to describe the ion-electron interactions. The Perdew-Burke-Ernzerr (PBE) form of the generalized gradient approximation (GGA) was adopted to deal with the exchange and correlation function[19]. The valence electronic configurations are considered as $3d^2\ 4s^2$ for Ti, $4p^6\ 4d^5\ 5s^1$ for Mo, $5s^2\ 5p^2$ for Sn. For consistency and accuracy, the energy cutoff was set to be 450 eV with 11×11×11 Monkhorst-Pack k-point sampled for convergency after careful test. The Methfessel-Paxton method (ismear=1) was used to obtain the accurate atomic positions, while the tetrahedron method with Blöchl corrections (ismear=–5) was employed to get accurate total energy and stresses. The energy convergence criterion was set to 10^{-6} eV/atom, and the maximum force per atom should be less than 10^{-2} eV/nm. The elastic constants can be estimated by calculating the stress tensors when applying a set of strains ($\varepsilon = \varepsilon_1, \varepsilon_2, \varepsilon_3, \varepsilon_4, \varepsilon_5, \varepsilon_6$) to the equilibrium lattice. The amount of the applied strain in the calculation of the stress tensors is about ±1%[20].

For the Ti-xMo-Sn systems, 16-atoms supercell with body-centered cubic (bcc) structure was used to simulate the β-phase. The concentration of Sn element was remained at 6.25% (1 atom), while Ti atom was progressively substituted by Mo atom in concentrations starting from Ti-1Mo-Sn (corresponding to 6.25%) up to Ti-5Mo-Sn (corresponding to 31.25%); the minimum composition variation of Mo is 6.25%, and the supercell models of Ti-xMo-Sn alloys are shown in Fig.1. The configuration of supercell with different

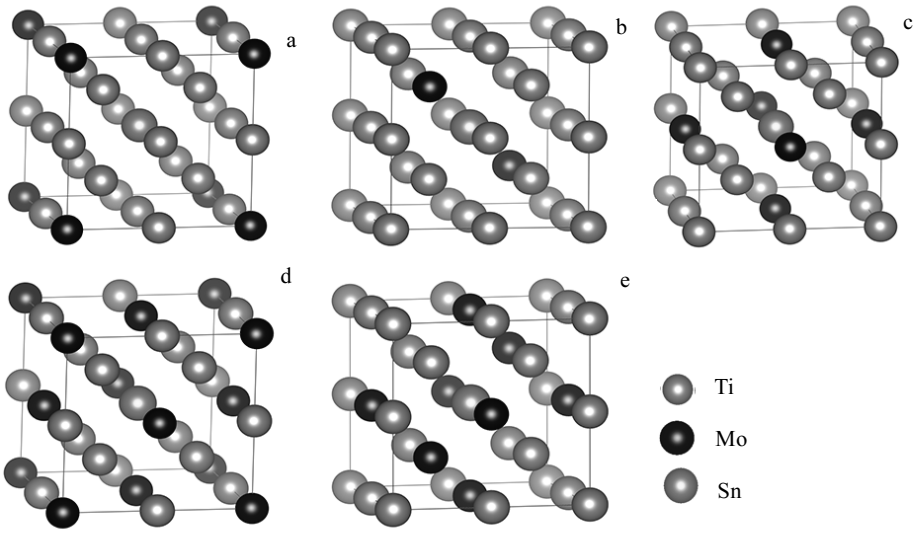

Fig.1 Supercell models of Ti-xMo-Sn alloys: (a) Ti-1Mo-Sn, (b) Ti-2Mo-Sn, (c) Ti-3Mo-Sn, (d) Ti-4Mo-Sn, and (e) Ti-5Mo-Sn

atomic positions has been tested to ensure the reasonableness and accuracy of Ti-*x*Mo-Sn(*x*=1~5) alloys. All concentrations in this paper were defined by atomic percentage. For each case, the geometrical optimization was always made first.

2 Results and Discussion

2.1 Structural and lattice properties

The lattice structure and atomic occupancy usually directly or indirectly determine the physical properties of materials in most cases. After complete geometry optimization, Ti-*x*Mo-Sn alloys still maintain the body-centered cubic structure because of the equivalent lattice constants. As shown in Fig.2, the lattice parameters *a* and unit cell volume V_0 of Ti-*x*Mo-Sn alloys are gradually reduced with increasing the Mo concentration. This is due to the fact that the atomic radius of Mo (0.140 nm) is smaller than that of Ti (0.147 nm), which causes the lattice shrink around the Mo atoms and increases the distortion of crystal lattice.

Young's modulus is an intrinsic characteristic of materials which depends on the type of crystal lattice. The cohesive energy E_{coh} and formation energy E_f were considered to determine the β phase stability of Ti-*x*Mo-Sn alloys with increasing the Mo concentration. As we know, the thermodynamic stability of β phase can be determined by the cohesive energy E_{coh}, while the metallurgical tendency to form a solid solution depends on the formation energy E_f. The larger negative formation energy and cohesive energy suggest that it is easier to form Ti-*x*Mo-Sn alloys with β phase solid solution in the experiment. The formation energy and cohesive energy can be described by following equation:

$$E_{coh}=\frac{1}{N_{total}}\left[E_{total}-N_{Ti}\cdot E_{Ti}^{atom}-N_{Mo}\cdot E_{Mo}^{atom}-N_{Sn}\cdot E_{Sn}^{atom}\right] \quad (1)$$

$$E_f=\frac{1}{N_{total}}\left[E_{total}-N_{Ti}\cdot E_{solid}^{Ti}-N_{Mo}\cdot E_{solid}^{Mo}-N_{Sn}\cdot E_{solid}^{Sn}\right] \quad (2)$$

where E_{total} is the total energy of supercell; E_{Ti}^{atom}, E_{Mo}^{atom} and E_{Sn}^{atom} are the energy of isolated atom of Ti , Mo and Sn, respectively; E_{solid}^{Ti}, E_{solid}^{Mo} and E_{solid}^{Sn} are the energy of Ti, Mo, Sn atom with equilibrium lattice parameter, respectively; N_{total}, N_{Ti}, N_{Mo} and N_{Sn} are the number of total atoms, Ti atoms, Mo atoms and Sn atom in supercell, respectively.

The calculated cohesive energy E_{coh}, formation energy E_f and average valence electron concentration *e*/*a* of Ti-*x*Mo-Sn alloys are listed in Table 1. The negative E_{coh} and E_f suggest that all these compounds can maintain the thermodynamic stability of β phase solid solution at 0 K. The decrease of E_{coh} indicates that the β phase of Ti-*x*Mo-Sn alloys becomes more stable with Mo addition. The average valence electron concentration *e*/*a* gives an empirical criterion for determining the phase composition of Ti alloys[14]. The transition phases in Ti-Mo alloys (such as α', α'' and ω) can be predicted when $e/a\approx4.13$, while β phase becomes dominant when $e/a \geq 4.2$[21]. It can be seen from Table 1 that the average valence electron concentration *e*/*a* for Ti-*x*Mo-Sn alloys is in the range of 4.13~4.63. It can be inferred that Ti-Mo-Sn alloy may induce the martensitic transformation with 6.25at% Mo addition, while β phase becomes dominant when Mo concentration is larger than 12.5at%, which is in good agreement with experimental and theoretical data [14].

2.2 Elastic properties

In an effort to obtain the influence of Mo concentration on the mechanical properties of Ti-*x*Mo-Sn alloys, the elastic moduli (bulk modulus *B*, shear modulus *G* and Young's modulus *E*), Poisson's ratio *v* and anisotropy factor *A* of Ti-*x*Mo-Sn alloys are discussed. The Young's modulus along three crystallographic directions (<100>, <110> and <111>) are estimated as well. The calculated elastic constants C_{ij} are listed in Table 2. Due to lack of experimental data of elastic constants, we only discuss the corresponding elastic properties in this calculation condition. For body-centered cubic (bcc) lattice, there are 3 independent elastic constants C_{11}, C_{12} and C_{44}. It can be seen from Table 2 that all these alloys satisfy the Born stability criteria for mechanical stability for bcc structure: $C_{11}>0$, $C_{44}>0$, $C_{11}-C_{12}>0$, $C_{11}+2C_{12}>0$ [22], meaning that all these alloys can maintain the mechanical stability of β phase. According to Ref.[23,24], the Cauchy pressure $C_{12}-C_{44}$ is related to the bonding characteristic in crystal lattice which can be used to analyze the ductile or brittle behavior of a material. The positive Cauchy pressure indicates more metallic character, while the negative $C_{12}-C_{44}$ stands for more covalent bonding characteristic. As shown in Table 2, the positive $C_{12}-C_{44}$ indicates that Ti-*x*Mo-Sn alloys show more metal characteristics with increasing the Mo concentration, which also has a positive effect on improving ductility.

The bulk modulus *B*, shear modulus *G* and Young's modulus *E* can be estimated from elastic constants by the Voigt-Reuss-Hill method, described as follows[25,26]:

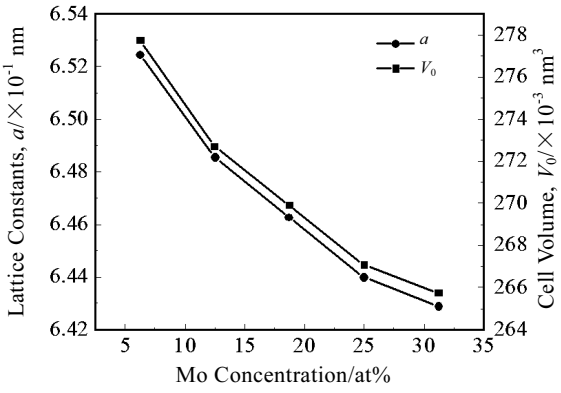

Fig.2 Calculated lattice constants *a* and cell volume V_0 of Ti-*x*Mo-Sn alloys

Table 1 Calculated formation energy E_f, cohesive energy E_{coh}

and valence electron concentration *e*/*a* of Ti-*x*Mo-Sn (*x* =1~5) alloys

Alloy	E_f/kJ·mol^{-1}	E_{coh}/kJ·mol^{-1}	*e*/*a*
Ti-1Mo-Sn (6.25at% Mo)	−14.0865	−521.8351	4.13
Ti-2Mo-Sn (12.5at% Mo)	−9.3750	−524.1927	4.25
Ti-3Mo-Sn (18.75at% Mo)	−10.2115	−528.4955	4.38
Ti-4Mo-Sn (25at% Mo)	−14.2885	−537.8411	4.50
Ti-5Mo-Sn (31.25at% Mo)	−11.2308	−545.5646	4.63

$$E = 9BG/(3B+G) \quad (3)$$

$$B = 1/2\ (B_v + B_R) \quad (4)$$

$$G = 1/2\ (G_v + G_R) \quad (5)$$

$$B_v = B_R = (C_{11} + 2C_{12})/3 \quad (6)$$

$$G_v = (C_{11} - C_{12} + 3C_{44})/5 \quad (7)$$

$$G_R = 5C_{44}(C_{11} - C_{12})/4C_{44} + (C_{11} - C_{12}) \quad (8)$$

where B_v, G_v are the bulk modulus and shear modulus calculated by Voigt approximation method, respectively; B_R, G_R are the bulk modulus and shear modulus calculated by Reuss approximation method, respectively.

The predicted bulk modulus *B*, shear modulus *G* and Young's modulus *E* are listed in Table 3 and visualized in Fig.3. It is well known that the bulk modulus *B* and shear modulus *G* can be employed to measure the resistance of alloys against the volume deformation and shape deformation, respectively[27, 28]. As shown in Fig.3, Mo is more effective in enhancing the ability of Ti-*x*Mo-Sn alloys to resist volume deformation, while the trend of shear modulus suggests that the characteristics of resisting shear deformation increase after an initial decrease with increasing the Mo concentration. The shear modulus *G* is more susceptible to Mo concentration in comparison with bulk modulus *B*. The Young's modulus *E* can reveal the stiffness of Ti-*x*Mo-Sn alloys which tends to decrease at the initial stage and then increase with Mo addition. The change tendency of the elastic modulus indicates that the shear modulus is the major contributor for reducing the Young's modulus. It is worth noting that the Young's modulus *E* of Ti-3Mo-Sn is only 48.47 GPa, which is perceived to be a promising material for orthopedic implant applications.

Table 2 Calculated elastic constants C_{11}, C_{12}, C_{44}, Cauchy pressure $C_{12}-C_{44}$, tetragonal shear constant C' of β phase in Ti-*x*Mo-Sn alloys

Alloy	C_{11}	C_{12}	C_{44}	$C_{12}-C_{44}$	C'
Ti-1Mo-Sn (6.25at% Mo)	143.36	99.96	50.56	49.40	21.70
Ti-2Mo-Sn (12.5at% Mo)	139.37	115.25	45.02	70.23	12.06
Ti-3Mo-Sn (18.75at% Mo)	137.85	127.42	32.55	94.87	5.215
Ti-4Mo-Sn (25at% Mo)	164.49	127.01	42.01	85.00	18.74
Ti-5Mo-Sn (31.25at% Mo)	191.44	132.35	48.97	83.38	29.54

Table 3 Calculated bulk modulus *B*, shear modulus *G*, Young's modulus *E*, Pugh ratio *B*/*G*, Poisson's ratio *v* and anisotropy factor *A* of β phase in Ti-*x*Mo-Sn alloys from the Voigt-Reuss-Hill method

Alloy	*B*/GPa	*G*/GPa	*E*/GPa	*B*/*G*	*v*	*A*
Ti-1Mo-Sn (6.25at% Mo)	114.43	41.84	111.88	2.73	0.34	2.33
Ti-2Mo-Sn (12.5at% Mo)	123.29	29.21	81.22	4.22	0.39	3.73
Ti-3Mo-Sn (18.75at% Mo)	130.90	16.84	48.45	7.77	0.44	6.24
Ti-4Mo-Sn (25at% Mo)	139.50	35.50	98.18	3.93	0.38	2.24
Ti-5Mo-Sn (31.25at% Mo)	152.04	48.97	132.66	3.10	0.35	1.66

The tetragonal shear constant C' and valence electron concentration *e*/*a* can be used as an empirical criterion to predict the low Young's modulus of β Ti alloys[13,14]. We also evaluated the relationship between Young's modulus and tetragonal shear constant C' or valence electron concentration *e*/*a* in Ti-*x*Mo-Sn alloys. As shown in Fig.4, the smaller tetragonal shear constant C' may induce the lower Young's modulus characteristics, the valence electron concentration criterion for designing the lowest Young's modulus of Ti-*x*Mo-Sn alloys should be in the range of 4.25 to 4.38. This may provide another perspective for designing Ti-Mo based alloys.

Ductility is a key parameter of materials when it comes to industrial applications, which can be revealed by Pugh ratio *B*/*G* and Poisson's ratio *v*. The alloys exhibit ductility when *B*/*G*>1.75 or Poisson's ratio *v*>0.26. The larger *v* or *B*/*G* of alloys suggest the better ductility. The Poisson's ratio *v* is given by[29]

$$v = (3B - E)/6B \quad (9)$$

The calculated Pugh ratio (*B*/*G*) and Poisson's ratio *v* are

listed in Table 3. All these alloys satisfy the criteria for ductile materials with the B/G>1.75 and Poisson's ratio v>0.26, indicating that all these alloys possess good ductility. With increasing the Mo concentration, the ductility of Ti-Mo-Sn alloys behaves opposite tendency compared to Young's modulus. It can be noticed that Ti-3Mo-Sn possesses the lowest Young's modulus and shows the best ductility in comparison with other Ti-xMo-Sn alloys. For the judgment of brittleness or ductility of Ti-xMo-Sn alloys, the Pugh ratio B/G and Poisson's ratio criterion show the same result with the Cauchy pressure criterion.

2.3 Elastic anisotropy in Ti-xMo-Sn alloy systems

The Young's modulus of β-Ti alloys usually exhibits an obvious anisotropic characteristics in different crystallographic directions. Tane et al found that the TNTZ (Ti-29Nb-13Ta-4.6Zr) alloy shows the lowest Young's modulus in <100> direction[30]. Moreover, it is reported that the anisotropy of Young's modulus may induce the texture and microcracks during processing[31]. Zener introduced an anisotropic factor A to quantify the anisotropy of cubic crystals[32]:

$$A = 2C_{44}/(C_{11} - C_{12}) \quad (10)$$

The calculated anisotropy factor A of Ti-xMo-Sn alloys is listed in Table 3. The calculated Young's modulus of Ti-xMo-Sn alloys along three crystallographic directions (<100>, <110> and <111>) is shown in Fig.5. It is clear that the Ti-xMo-Sn alloys exhibit an obvious anisotropic characteristic which is obviously dependent on Mo concentration. The elastic anisotropy of these alloys increases at first and then decreases with Mo addition, and Ti-3Mo-Sn alloy exhibits the highest anisotropic characteristic compared to other alloys. It is worth noting that the Ti-xMo-Sn alloys oriented in the <100> crystallographic direction always show the lowest Young's modulus, while the highest Young's modulus is along the <111> crystallographic direction. The tendency of anisotropy is proportional to ductility with increasing the Mo concentration, indicating that the increased ductility may lead to higher anisotropy in Ti-xMo-Sn alloys.

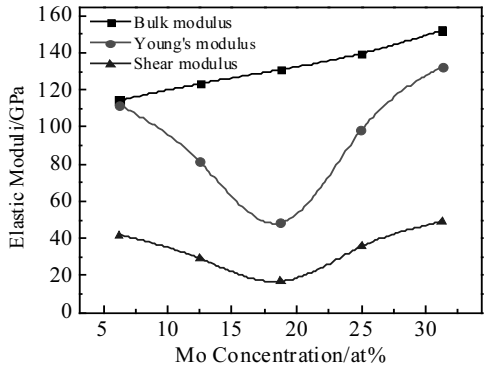

Fig.3 Predicted trends in the elastic properties of β phase in Ti-xMo-Sn alloys based on the calculated elastic constants C_{ij}

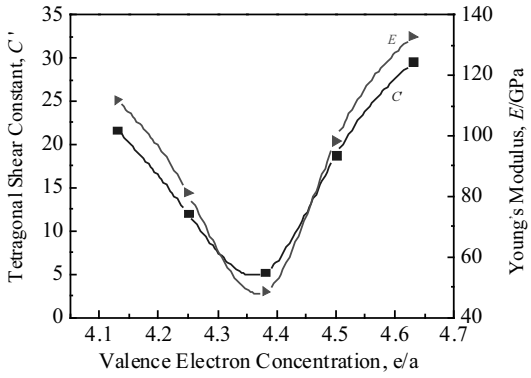

Fig.4 Variation of calculated Young's modulus E and tetragonal shear constant C' with valence electron concentration of β phase in Ti-xMo-Sn alloys

2.4 Electronic properties

In order to reveal the mechanism of β-phase stability from bonding character perspective, we calculated the total density of states (DOS) and partial density of states (PDOS) of Ti-xMo-Sn alloys with Mo addition, as visualized in Fig.6. The vertical dotted black line indicates the Fermi level. The Fermi level is the boundary between valence electrons and free electrons, and the valence electrons of metallic materials are generally distributed below the Fermi level. For all cases, the total and partial DOS cross the Fermi level, suggesting that no energy gap exists at the Fermi level. It can be inferred from Fig.6 that the bonding state is mainly in the energy range between –9 eV and 0 eV, mainly occupied by 4s, 3p and 3d states of Ti, 5s, 4p, 4d states of Mo and 5s, 5p states of Sn. For easier visualization and analysis, we only mark the main valence electron contribution orbitals of Ti, Mo, Sn atoms in Fig.6. The structural stability of alloys is associated with its bonding electrons around the Fermi level[33]. For Ti-xMo-Sn alloys, the total DOS at the Fermi level decreases gradually with increasing the Mo concentration, and the electrons move toward the lower energy levels, meaning that Ti-xMo-Sn alloys become more stable with Mo addition. Ti-3d and Mo-4d states have a strong hybridization in the energy range between –4.5 eV and 3 eV. With increasing the Mo concentration, the peak height of Ti atom declines while the peak height of Mo atom rises, increasing the bonding and hybridization between Ti-3d and Mo-4d states. In addition, the wide band at –9 eV and –7 eV is related to Sn atom, and the peak height of Sn atom is almost unchanged, indicating that the β-phase stability of Ti-xMo-Sn alloys is mainly determined by Mo element. The valence electrons of Sn-5s orbit have weak hybridization with Ti-3d and Mo-4d orbits due to the Sn-Sn pairs electrons, and this has been nicely illustrated in Ref.[34]. All of the above behavior indicates that the stability of Ti-xMo-Sn alloys can be promoted by increasing the Mo content, in consistent with the previous cohesive energy results.

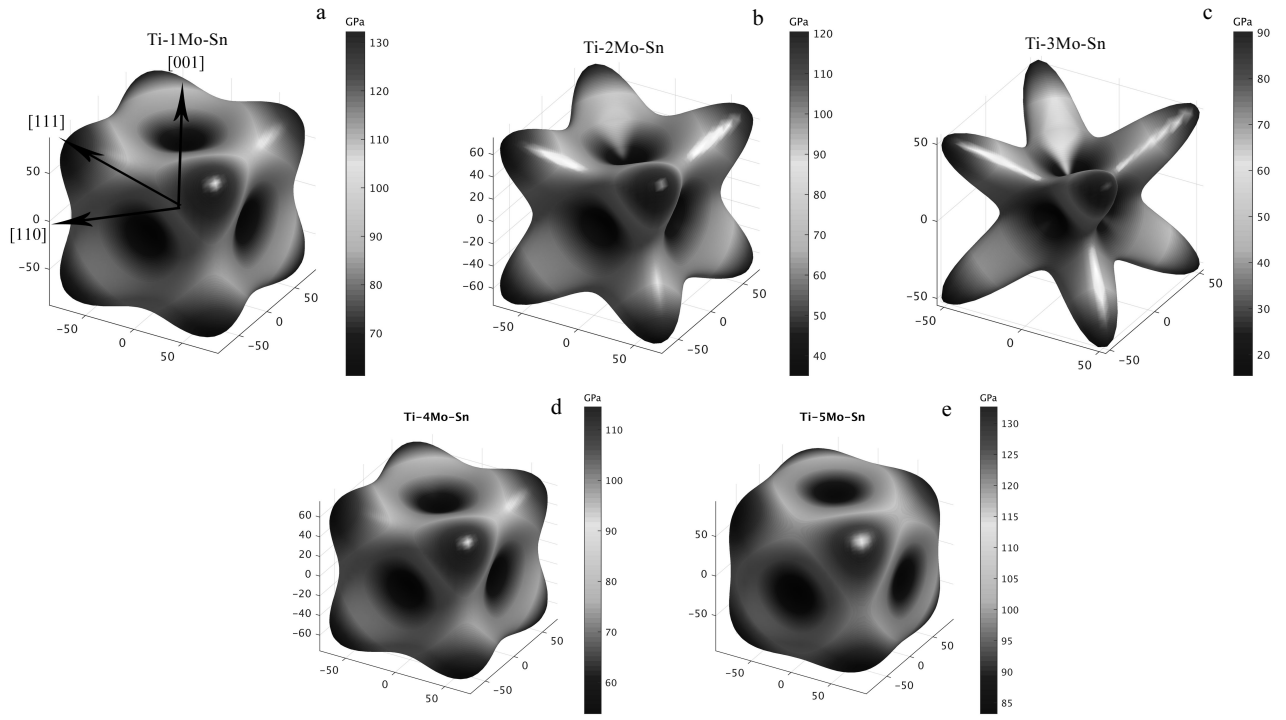

Fig.5 Calculated Young's modulus of β phase in Ti-xMo-Sn alloys along three crystallographic directions (<100>, <110> and <111>): (a) Ti-1Mo-Sn, (b) Ti-2Mo-Sn, (c) Ti-3Mo-Sn, (d) Ti-4Mo-Sn, and (e) Ti-5Mo-Sn

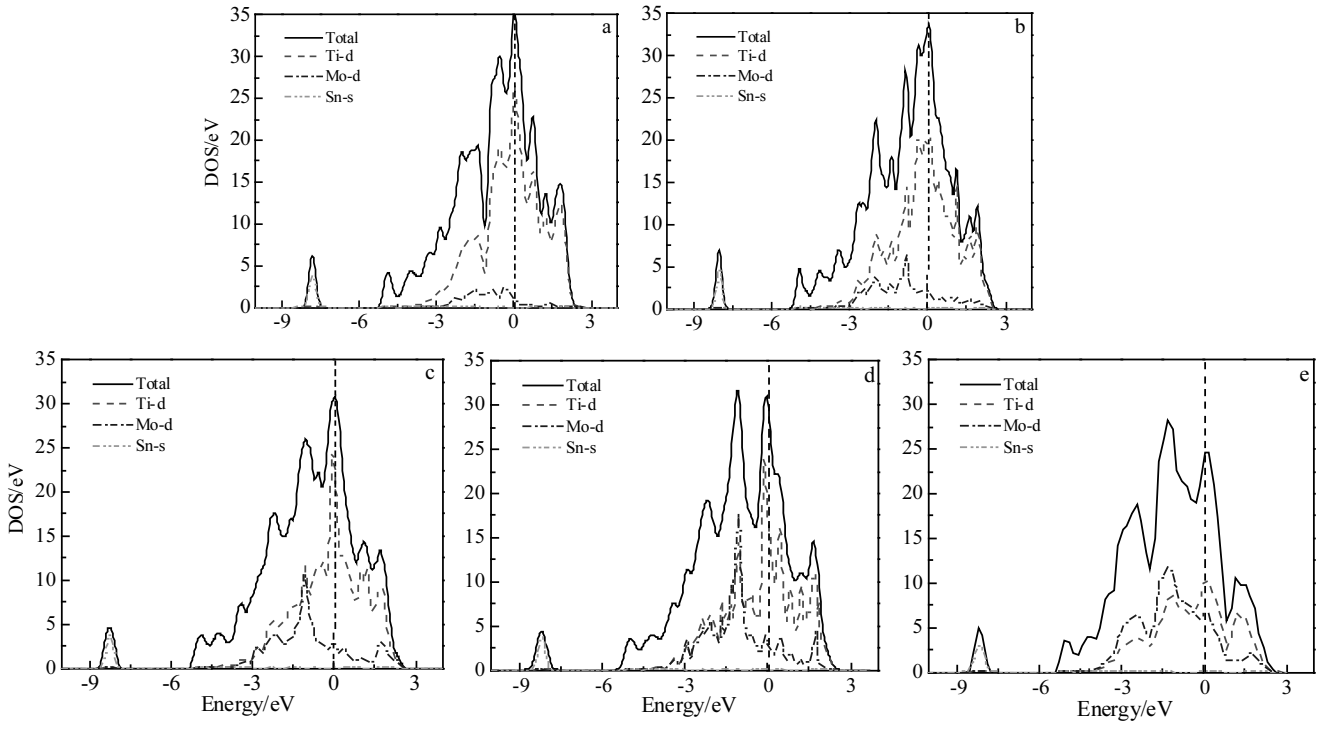

Fig.6 Calculated total DOS and partial DOS for Ti-xMo-Sn alloys: (a) Ti-1Mo-Sn, (b) Ti-2Mo-Sn, (c) Ti-3Mo-Sn, (d) Ti-4Mo-Sn, and (e) Ti-5Mo-Sn (vertical dotted black line indicates the Fermi level)

3 Conclusions

1) The β-phase stability of Ti-xMo-Sn alloys can be enhanced by Mo addition.

2) The elastic properties of Ti-xMo-Sn alloys are predicted by the Voigt-Reuss-Hill approximation. The bulk modulus B increases with Mo addition, while the shear modulus G and Young's modulus E decrease at first and then increase. The lowest Young's modulus is always oriented in the <100> crystallographic direction and the valence electron concentration e/a criterion for low Young's modulus Ti-Mo based alloys should be in the range of 4.25 to 4.38. The Pugh ratio B/G and Poisson's ratio v indicate that all these alloys perform ductility. Ti-3Mo-Sn alloy possesses the lowest Young's modulus (48.47 GPa) and the best ductility, showing great potential in biomedical applications.

3) The enhancement of β-phase stability is attributed to the bonding and hybridization between Ti-3d and Mo-4d states, while Sn-5s orbit has a weak hybridization with Ti-3d and Mo-4d orbits.

References

1 Long Marc, Rack H J. *Biomaterials*[J], 1998, 19(18): 1621

2 Zhu Kangping, Zhu Jianwen, Qu Henglei. *Rare Metal Materials & Engineering*[J], 2012, 41(11): 2058

3 Webster T J, Ejiofor J U. *Biomaterials*[J], 2004, 25(19): 4731

4 Garcíaalonso M C, Saldaña L, Vallés G *et al*. *Biomaterials*[J], 2003, 24(1): 19

5 Thompson G J, Puleo D A. *Biomaterials*[J], 1996, 17(20): 1949

6 Muhammad Farzik Ijaz, Denis Laillé, Lorène Héraud *et al*. *Materials Letters*[J], 2016, 177: 39

7 Li Peiyou, Ma Xindi, Tong Ting *et al*. *Journal of Alloys and Compounds*[J], 2020, 815: 152 412

8 Ma Xiqun, Niu Hongzhi, Su Yongjun *et al*. *Rare Metal Materials and Engineering*[J], 2019, 48(10): 3095

9 Masaki Tahara, Kazuya Hasunuma, Ryosuke Ibaki *et al*. *Advanced Engineering Materials*[J], 2019, 21(11): 1 900 416

10 Sochacka P, Miklaszewski A, Jurczyk M. *Journal of Alloys and Compounds*[J], 2019, 776: 370

11 Biesiekierski A, Wang J, Gepreel M A *et al*. *Acta Biomaterialia*[J], 2012, 8(5): 1661

12 Karre R, Niranjan M K, Dey S R. *Materials Science and Engineering C*[J], 2015, 50: 52

13 Hideaki Ikehata, Naoyuki Nagasako, Tadahiko Furuta *et al*. *Physical Review B*[J], 2004, 70(17): 3352

14 Li You, Song Xiping. *Materials Letters*[J], 2012, 80: 165

15 Mohamed Abdel-Hady, Keita Hinoshita, Masahiko Morinaga. *Scripta Materialia*[J], 2006, 55(5): 477

16 Zhou Yinglong, Luo Dongmei. *Materials Characterization*[J], 2011, 62(10): 931

17 Chen Xiaoxue, Guo Shun, Zhao Xinqing. *Materials Science Forum*[J], 2013, 748: 855

18 Hafner J. *Journal of Computational Chemistry*[J], 2010, 29(13): 2044

19 John P Perdew, Kieron Burke, Matthias Ernzerhof *et al*. *Physical Review Letters*[J], 1997, 77(18): 3865

20 Yvon Le Page, Paul Saxe. *Physical Review B*[J], 2002, 65(10): 104 104

21 Luke C A, Taggart R, Polonis D H. *Journal of Nuclear Materials*[J], 1965, 16(1): 7

22 Frederick Milstein. *Physical Review B*[J], 1970, 2(2): 512

23 Zhang Hualei, Sun Xun, Lu Song *et al. Acta Materialia*[J], 2018, 155: 12

24 Thompson R P, Clegg W J. *Current Opinion in Solid State and Materials Science*[J], 2018, 22(3): 100

25 Niranjan M K. *Intermetallics*[J], 2012, 26(7): 150

26 Benkaddour K, Chahed A, Amar A *et al*. *Journal of Alloys and Compounds*[J], 2016, 687: 211

27 Xie Y, Yu H T, Yi T F *et al*. *Applied Materials & Interfaces*[J], 2014, 6(6): 4033

28 Sun Shiyang, Xu Pingping, He Yonghong *et al*. *Rare Metal Materials and Engineering*[J], 2018, 47(1): 108

29 Paul S Nnamchi, Obayi C S, Iain Todd *et al*. *Journal of the Mechanical Behavior of Biomedical Materials*[J], 2016, 60: 68

30 Tane M, Akita S, Nakano T *et al*. *Acta Materialia*[J], 2008, 56(12): 2856

31 Shivakumar I Ranganathan, Ostoja Starzewski Martin. *Physical Review Letters*[J], 2008, 101(5): 55 504

32 Zener C M, Siegel S. *Journal of Physical and Colloid Chemistry*[J], 1949, 53(9): 1468

33 Hoffman R. *Solids and Surfaces: A Chemist's View of Bonding in Extended Structures*[M]. New York: VCH Publishers, 1988

34 Gutiérrez-Moreno J J, Guo Y, Georgarakis K *et al*. *Journal of Alloys and Compounds*[J], 2014, 615: 676

医用低模量 Ti-Mo-Sn 合金的第一性原理计算

赵　曦[1,2]，余　森[1,2]，郑继明[3]，刘汉源[1,2]，程　军[1,2]，麻西群[1,2]

(1. 西北有色金属研究院，陕西 西安 710016)

(2. 陕西省医用金属材料重点实验室，陕西 西安 710016)

(3. 西北大学，陕西 西安 710069)

摘　要：采用基于密度泛函理论的第一性原理计算方法，研究了 Mo 含量对 Ti-*x*Mo-Sn(*x*=1~5)合金相稳定性、弹性性质及其电子结构的影响，采用 Voigt-Reuss-Hill 近似方法估算了体系的多晶弹性模量，提出了低模量 Ti-Mo-Sn 合金的价电子准则，为医用钛合金的设计提供了理论基础。结果表明：Mo 元素合金化能明显提高 Ti-*x*Mo-Sn 合金的 β 相稳定性，所有合金都满足力学稳定性要求，随 Mo 元素含量增加，合金的体积模量 *B* 逐渐变大，而剪切模量 *G* 和杨氏模量 *E* 先减小后增大，其中 Ti-3Mo-Sn 具有最低的杨氏模量（48.47 GPa）和最佳的延展性，在生物医用领域展现出巨大潜力。Ti-*x*Mo-Sn 合金的弹性各向异性 *A* 与 Mo 元素含量有关，低弹性模量取向始终沿<100>晶体学方向。最后，结合 Ti 合金的总态密度（DOS）和分波态密度(PDOS)分析讨论了 Mo 元素对 β 相结构稳定性的影响机制。

关键词：医用钛合金；第一性原理计算；合金设计；低弹性模量；弹性性能

作者简介：赵　曦，女，1992 年生，硕士，西北有色金属研究院，陕西 西安 710016，电话：029-86222297，E-mail: zhao_xii@163.com